Journal of Engineering Issues and Solutions

Seismic Assessment of a Masonry Building in Patan, Nepal

Abiskar Acharya[1,*], Alok Dahal[2], Aashutosh Kumar Jha[3], Angel Mainali[4], Amar Singh Thagunna[5], Asal Babu Pathak[6], Rabindra Adhikari[7]

[1,2,3,4,5,6]Department of Civil Engineering, Institute of Engineering, Thapathali Campus, Tribhuvan University, Kathmandu, Nepal

[7]Department of Civil Engineering, Institute of Engineering, Pulchowk Campus, Tribhuvan University, Kathmandu, Nepal

**Corresponding email: acharya.abiskar7@gmail.com*

Received: November 25, 2025; Revised: 27 January, 2026; Accepted: March 21, 2026

Abstract

Nepal's cultural heritage, especially the traditional masonry structures found in UNESCO World Heritage sites like Patan, is seriously threatened by the country's high seismicity. Many of these buildings were constructed using pre-code methods, such as unreinforced brick masonry with mud mortar, which made them extremely vulnerable to the 2015 Gorkha earthquake. The actual as-built conditions and structural behavior of such heritage buildings are frequently not reflected in Nepal's current seismic risk models. By conducting a thorough seismic performance evaluation of a typical traditional brick building in Patan, this study fills this gap. Laboratory testing was used to determine the brick's compressive strength, and field surveys were utilized for the case study's selection and geometric characterization. Nonlinear static pushover analyses were performed in the two principal directions using a three-dimensional finite element model created in DIANA FEA 10.5. With a base shear of 410 kN at an ultimate displacement of 36.5 mm in the X-direction and 236 kN at 65.5 mm in the Y-direction, the results show a strong directional dependence of seismic capacity. Fundamental periods of 0.594 and 0.388 seconds were found by eigen value analysis. Four damage states were linked to roof displacement through the development of fragility curves. Analysis using the Capacity Spectrum Method against NBC 105:2020 demand spectra shows extremely high vulnerability, with collapse expected under stronger shaking and collapse prevention limits exceeded at PGA levels as low as 0.1g. For Patan's traditional masonry buildings, the results offer vital, region-specific fragility and capacity data that support well-informed risk mitigation, retrofitting techniques, and heritage conservation planning.

Keywords: *Seismic Vulnerability, Pushover Analysis, Capacity Spectrum Method, Fragility Assessment, Traditional Masonry*

1. Introduction

1.1 Seismic Hazard in Nepal and Vulnerability of Traditional Masonry

Nepal's geographical position, defined by the collision between the Indian and Eurasian tectonic plates at an approximate convergence rate of 40-50 mm per year (Jade et al., 2014), subject the region to frequent and intense seismic phenomena. The country is located in a tectonically active area that has a number of major fault lines whose overall distribution adds significantly to the seismic risk in the area, as shown in Figure 1. This continuous tectonic action leads to crustal strain, which is periodically discharged with the help of large earthquakes. This risk is highlighted by historical seismicity; The most notable occurrences in the recent past have been the 2015 Gorkha (Mw 7.8) and the 2023 Jajarkot (Mw 6.4) earthquakes. The Gorkha event in 2015 brought with it a strong socioeconomic effect, with an estimated 8,790 deaths, 22,300 injuries, and over half a million houses destroyed (Lizundia et al., 2016). These incidents highlight the importance of proper seismic risk management measures in order to mitigate any future losses.

Table 1: Major Historical Earthquakes in Nepal and Their Impacts

Event / Location	Date	Magnitude (Mw)	Key Impacts (Fatalities, Injuries, and Damage)	Source
Gorkha Earthquake	April 25, 2015	7.8	Approx. 9,000 fatalities, >22,000 injuries, ~1 million structures damaged or destroyed.	(National Planning Commission, 2015)
Gorkha Aftershock	May 12, 2015	7.3	>200 additional fatalities, >2,500 injuries, further damage to already weakened structures.	(Hayes et al., 2017)
Jajarkot Earthquake	November 3, 2023	6.4	154 fatalities, 366 injuries, >62,000 houses damaged.	(IFRC, 2023)
Udayapur Earthquake	August 20, 1988	6.6	>720 fatalities, thousands injured, >65,000 buildings damaged.	(Fujiwara et al., 1988)
Bajhang Earthquake	July 29, 1980	6.5	~200 fatalities, ~5,600 injured, >13,000 buildings destroyed.	(Khanal, 1997)

Note: Casualty and damage figures are based on reported estimates from the cited sources and may vary slightly between different reports.

Figure 1: Generalized map illustrating major tectonic fault lines contributing to seismic hazard in Nepal.

A world heritage site is a place that is designated by the United Nations Educational, Scientific, and Cultural Organization (UNESCO) as having universal significance to humans as a whole. The importance of these sites to the common interest of the current and future generations is attributed to their cultural or natural significance or a mixture of both**.** Nepal is rich in both cultural and natural heritage, and despite being a small country, it has four UNESCO World Heritage Sites, two of which are classified as natural and two as cultural. Traditional masonry constructions, particularly those situated within UNESCO World Heritage areas like Patan in the Kathmandu Valley, exhibit acute seismic vulnerability (Kiyono et al., 2017).

Table 2: Name of Heritage Sites in Nepal

Type	World Heritage Sites in Nepal
Cultural	Kathmandu Valley (Patan Durbar square and six other monument zones) Lumbini
Natural	Sagarmatha National Park Chitwan National Park

Structures often erected using pre-code standard building practices and materials, such as unreinforced mud-mortar brick masonry, have consistently demonstrated a high degree of fragility during past seismic events (Gautam et al., 2016). The Kathmandu Valley was designated as a UNESCO World Heritage Site in 1979 for its unique Newari culture that blends Buddhist and Hindu elements (UNESCO, 2018). It consists of palaces and residential structures that form the core of its historical and artistic identity. These structures typically employ locally sourced materials like brick, stone, and wood. These incorporates traditional Newari techniques such as *silay* mortar for water-resistant *Daci Appa* bricks, alongside mud mortar for unreinforced masonry walls (Adhikari et al., 2019; Combey et al., 2021; Gautam et al., 2016). Daci Appa bricks are traditional handmade bricks commonly used in Newar architecture of the Kathmandu Valley, Nepal. They are also known as "terracotta bricks" or locally as “Dachi Appa”, derived from the Newari language, where "Daci" means fired or baked and “Appa" means bricks.

Despite their architectural merit, these traditional methods often lack considerations for contemporary seismic design. It results in characteristics such as low tensile strength, inadequate connections between walls and floors, and susceptibility to material degradation, thereby rendering them exceptionally vulnerable to earthquake-induced stresses (Furukawa et al., 2017).

The 2015 Gorkha earthquake starkly revealed this vulnerability, causing extensive damage to historic buildings in Patan Durbar Square. Major losses included the Char Narayan Mandir and the monument of Yog Narendra Malla (Dey et al., 2015). A study by (Furukawa et al., 2017) on a 300-year-old, two-story masonry structure in Patan Durbar Square, identified the emergence of new cracks and a significant post-earthquake reduction in natural frequencies ranging from 3.46% to 11.86% and stiffness between 8.0% and 13.8%. Masonry buildings are the predominant structural form in urban centers like Patan. Data from the National Population and Housing Census, 2011, indicate that 44.21% of households in Nepal reside in dwellings constructed with mud-bonded brick foundation, while an additional 17.6% occupy houses with cement-bonded brick foundation. The census done in 2021 shows different results. The comparison of various foundation types in 2011 and 2021 is shown in Table 3. A substantial proportion of these buildings, particularly older constructions, do not comply with modern seismic regulations, a factor that increases their risk.

Table 3: Comparison of Nepal's Building Foundation type (2011 vs. 2021 Census)

Parameter / Main Construction Material	Value (2011)	Value (2021)	Trend
Total Households	5,427,302	6,666,937	+22.8%
Mud-Bonded Brick/Stone	44.21%	33%	Significant Decrease
Cement-Bonded Brick/Stone	17.6%	29.8%	Moderate Increase
RCC Pillar Houses	9.9%	22.4%	Major Increase

Source: National Population and Housing Census 2011, 2021

1.2 Need for Specific Vulnerability Assessment

Quantitative evaluation methodologies such as fragility functions are needed for effective seismic risk management. Fragility functions establish probabilistic correlations between seismic hazard intensity measures (IMs) and the likelihood of structural damage exceeding predefined limit states (Zentner et al., 2016). Some research in Nepal has focused on developing empirical fragility curves for common building typologies, such as low-rise reinforced concrete (RC) frame structures with masonry infill (Gautam & Chaulagain, 2016). These studies often rely on generalized assumptions that may not adequately capture the prevalent issues of inconsistent construction quality and poor use of seismic codes. As a result, the actual seismic performance of many buildings diverges from predictions based on code provisions or generalized empirical models, thereby compromising the accuracy of existing risk assessments.

Current seismic risk models for Nepal may not sufficiently represent the as-built conditions of structures. These models lack the specificity required for distinct heritage typologies, such as those found in Patan (Pan et al., 2018).There is an urgent necessity to develop fragility models that accurately capture the inherent weaknesses of traditional masonry and reflect their actual constructed circumstances. Related studies on similar structures in Bhaktapur have also highlighted the susceptibility of traditional masonry to failure due to inherent deficiencies in structural integrity and low tensile strength (Gautam & Rodrigues, 2021)

1.3 Objectives and Scope of the Study

This research endeavors to address the critical deficiency in seismic vulnerability assessment for Patan's heritage structures. The primary objectives are to: 1) select and characterize a representative pre-1934 unreinforced masonry building through detailed field investigations; 2) ascertain the mechanical properties of its constituent materials via laboratory testing; and 3) evaluate its seismic capacity and generate performance-based fragility curves by developing and analyzing a 3D finite element model. The findings are intended to provide quantitative tools to support targeted retrofitting and cultural heritage preservation initiatives.

2. Materials and Methods

The methodological framework adopted for this study incorporates a combination of field investigations and advanced computational modeling techniques. It comprehensively assesses the seismic performance of a characteristic traditional masonry building in Patan.

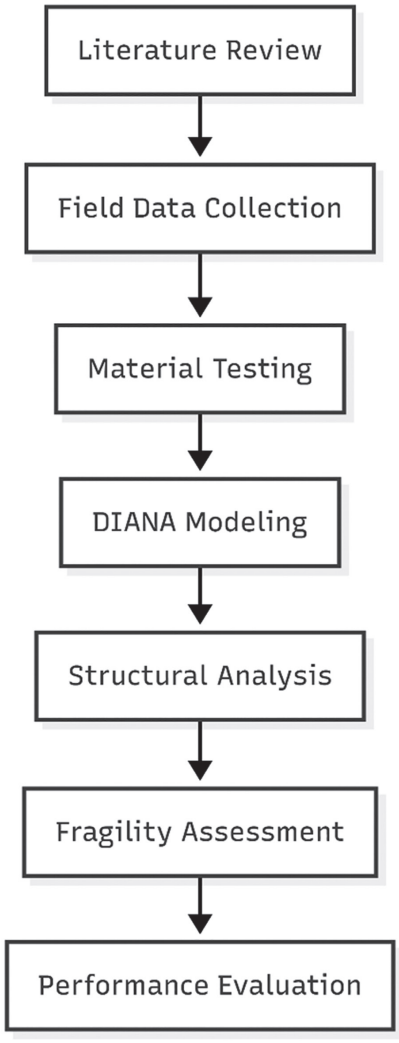

Figure 2: Research methodology workflow

2.1 Case Study Building: Selection and Description

2.1.1 Selection Criteria and Field Investigation

A representative structure was identified from the historic urban fabric of Patan, following a visual survey encompassing over 250 traditional brick structures. The selection process prioritized buildings that displayed distinctive structural and architectural features characteristic of Patan's older constructions. A particular focus was placed on those buildings utilizing mud mortar and unreinforced masonry techniques. The chosen building is situated approximately 100 meters from the Pimbahal area, a neighborhood of cultural significance. It was suitable as it aligned with the typical geometry, construction methodologies, and urban layout of masonry buildings present in the region. A pivotal criterion in its selection was its construction predating the 1934 Bihar-Nepal earthquake (Mw 8.2), rendering it representative of the traditional Newari architectural practices common within Patan's UNESCO World Heritage.

A field visit was conducted in December 2024 to systematically document the building's structural system, any visible patterns of damage, and to estimate its key dynamic properties. Due to the unavailability of precise damage records from the 1934 earthquake, an understanding of its historical performance was obtained by observing its current condition. Regional damage trends were also documented from subsequent seismic events, such as the 2015 Gorkha earthquake(Furukawa et al., 2017). The building's layout is characterized by exposure on three sides and attachment to an adjacent structure on the fourth. This reflects the typical Patan row housing typology, where buildings frequently share party walls while possessing distinct structural systems on their other elevations. Figure 3 illustrates the geographical location of the study building, and Figure 4 provides an external visual representation.

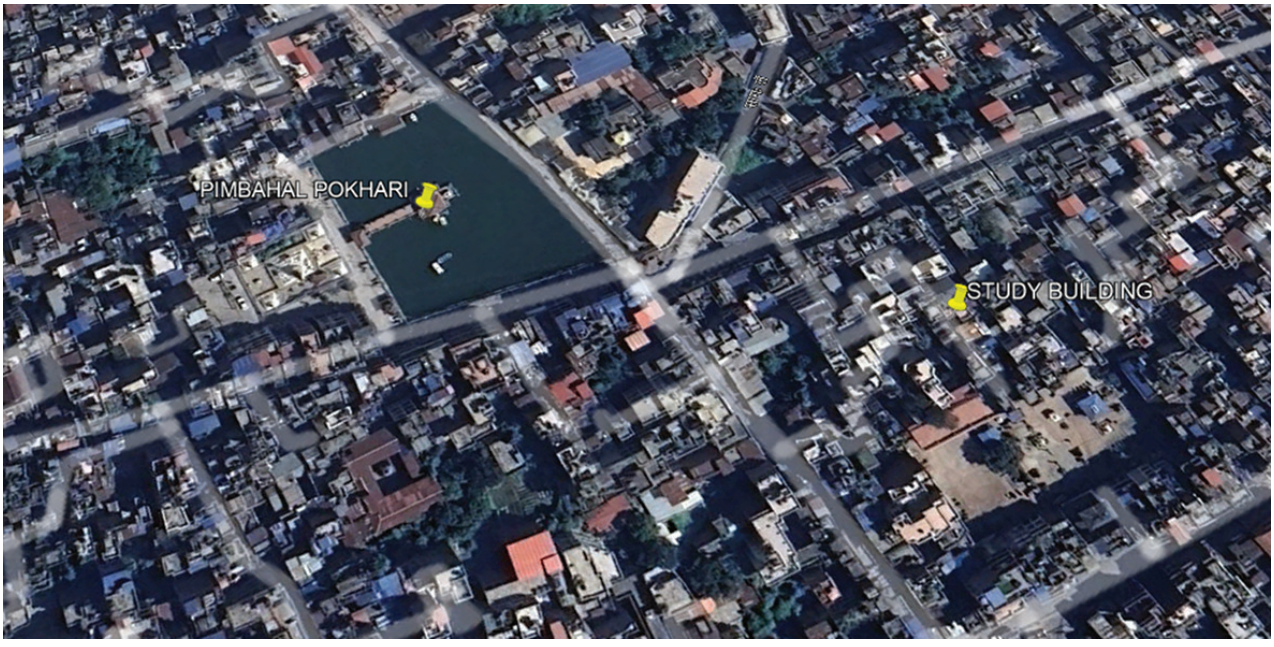

Figure 3: Location of the study building near Pimbahal Pokhari, Patan. (Source: Google Earth, adapted by authors)

Figure 4: External view of the selected pre-1934 traditional masonry building in Patan.

2.1.2 Structural and Architectural Characteristics

The selected structure is a 4.5-story unreinforced masonry building, configured with a rectangular plan that measures 2.52 meters in width (Y-direction) and 5.65 meters in length (X-direction). It possesses an overall height of 8.3 meters, resulting in an average story height of 1.85 meters. This average story height is less than the 2.20 to 2.50 meter range typically documented for traditional Newari homes within the Kathmandu Valley(Date et al., 2003). This variance could be attributed to a more compact architectural design, the presence of a partial top story such as an attic or rooftop enclosure, or differing conventions in measurement. The construction features brick masonry bonded with mud mortar. a technique characteristic of pre-1934 Newari buildings. These are recognized for their cultural importance, but also for their inherently low resistance to seismic forces(Gautam et al., 2016).

The walls are not the same thickness at all levels: the first three stories are built with 450 mm thick walls, and the final two stories have 300 mm thick walls. This common trend of making the wall thickness less as the level increases is mainly aimed at reducing the overall deadload. This may unintentionally result in a lower level of lateral load-carrying capacity and thus escalate the seismic vulnerability of the building. The structure lacks internal load-bearing brick walls; lightweight plywood partitions are employed to divide spaces in the upper rooms. This indicates that the perimeter walls function as the primary structural

components responsible for resisting both lateral and gravity-induced loads.

2.1.3 Urban Configuration and Construction Details

The structure lies in the historical town center of Patan, a region that can be characterized by tightly spaced row-house structures. Its structural design, with three free-standing sides and one that is attached to a neighboring structure, is common in urban planning where the limitation of space determines the interrelated structures of the building. Although the out-of-plane collapse is more prone to the free-standing elevations, which are inherently weaker, the shared party wall can provide a certain amount of lateral restraint during the seismic event (Furukawa et al., 2017). During the site visit, noticeable damage patterns, such as cracks and indications of material deterioration, were carefully recorded. These were exacerbated by the building's age and prior seismic activity, such as the 2015 Gorkha earthquake.

The building's construction displays traditional Newari methodologies, employing locally produced bricks bonded with mud mortar. This combination of materials, despite its cultural significance, contributes to the inherent seismic vulnerability of the structure. This is primarily due to its low tensile strength and weak cohesive properties when subjected to cyclic loading conditions(Gautam et al., 2016). In Patan, traditional buildings typically utilized mud mortar rather than cement or lime-based alternatives, a practice consistent with the construction techniques observed in this building and comparable heritage structures. The presence of plywood partitions in the upper levels, due to their minimal contribution to structural resistance, further diminishes the building's overall lateral stiffness.

A summary of the building's key characteristics is provided in Table 4, and the plan and the elevations are illustrated in Figures 5 to 9.

Table 4: Characteristics of the Selected Study Building

Parameter	Value	Notes
Plan Dimensions	5.65 m × 2.52 m	Rectangular plan, typical of Patan's row housing.
Total Height	8.3 m	Measured from ground to top, including all stories.
Number of Stories	4.5	4 full stories plus a partial top story (e.g., attic).
Average Story Height	~1.85 m	Lower than typical 2.20–2.50 m for Newari houses; may vary by floor.
Wall Thickness (Floors 1–3)	450 mm	Brick masonry with mud mortar, load bearing.
Wall Thickness (Floors 4–4.5)	300 mm	Reduced thickness in upper stories, frequent practice.
Internal Walls	None (brick); plywood in upper rooms	Lightweight partitions, non-load bearing.
Structural Configuration	One side adjacent, three sides free	Reflects row housing with shared party wall.
Construction Material	Brick with mud mortar	Pre-1934 Newari construction.
Location	~100 m from Pimbahal	Within Patan's historic urban core.

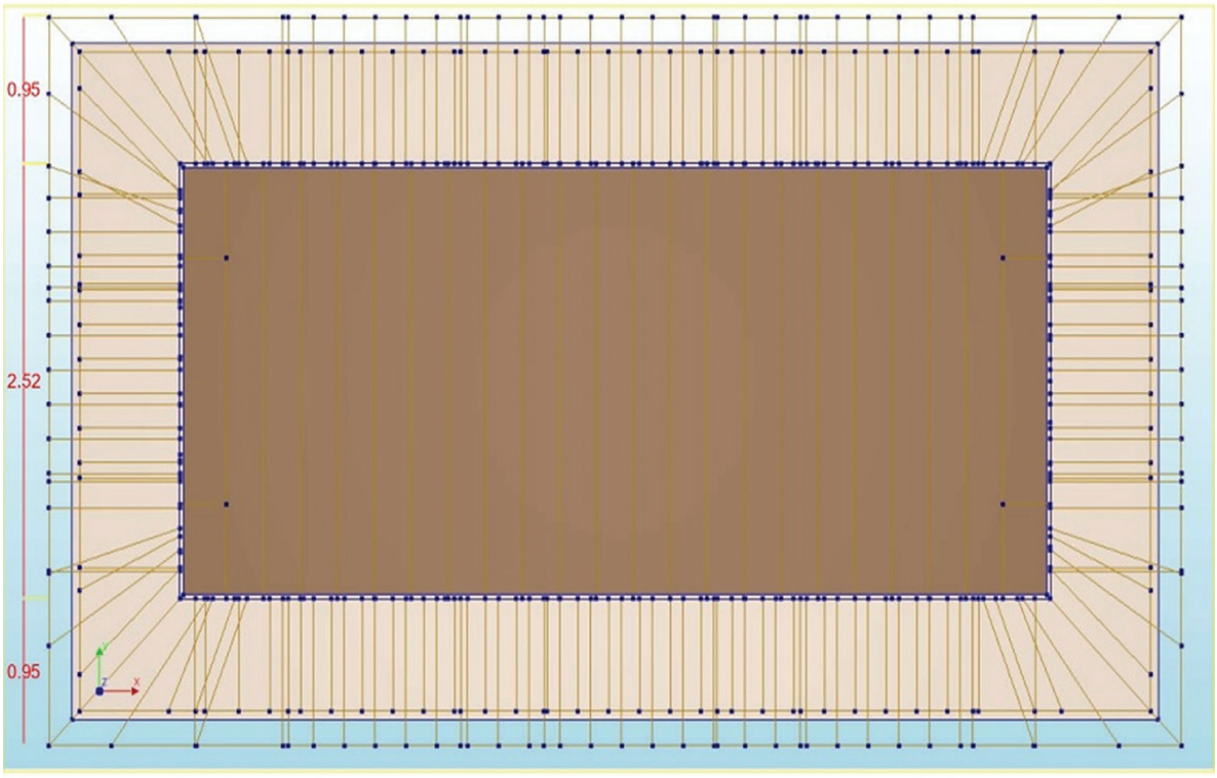

Figure 5: Plan View

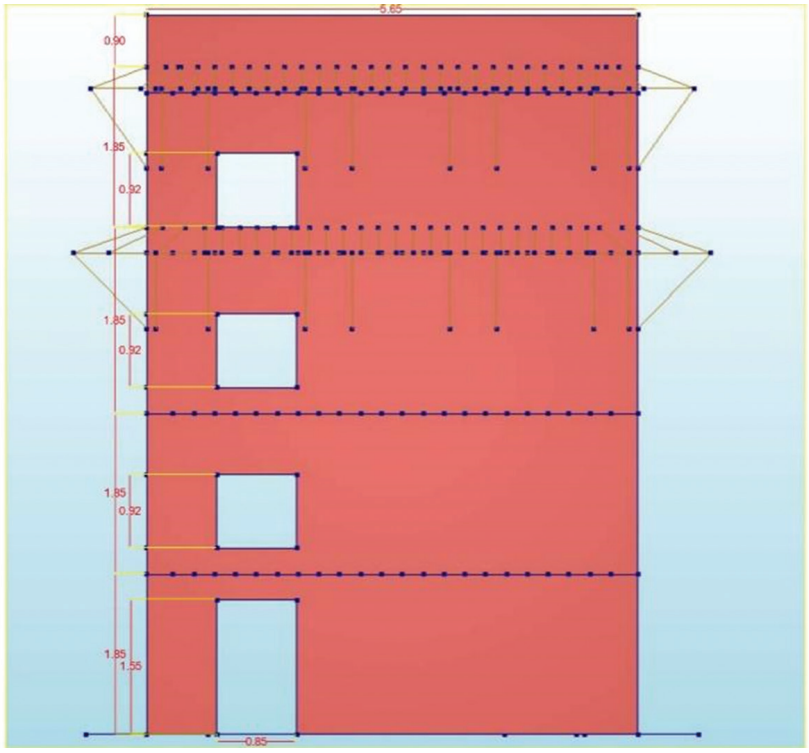

Figure 6: Front View

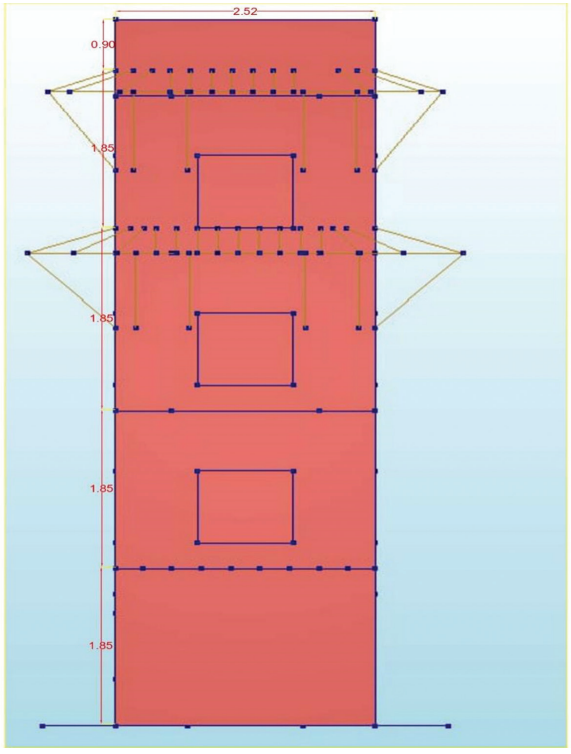

Figure 7: Left Side View

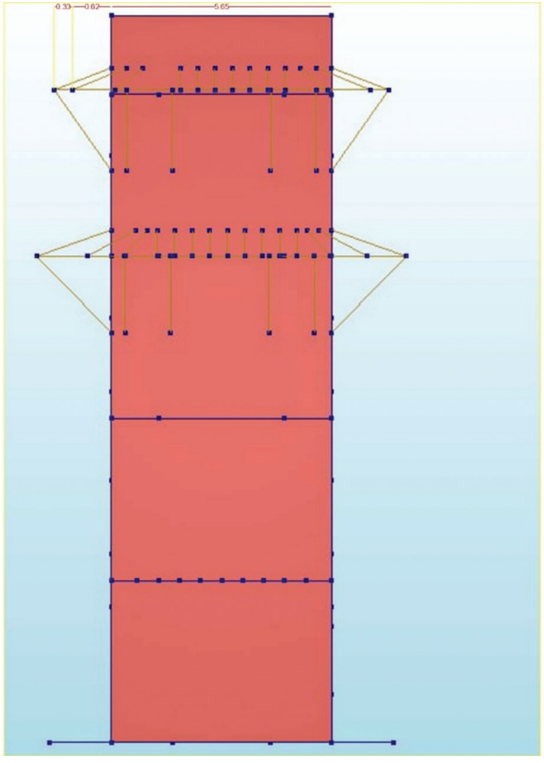

Figure 8: Right Side View

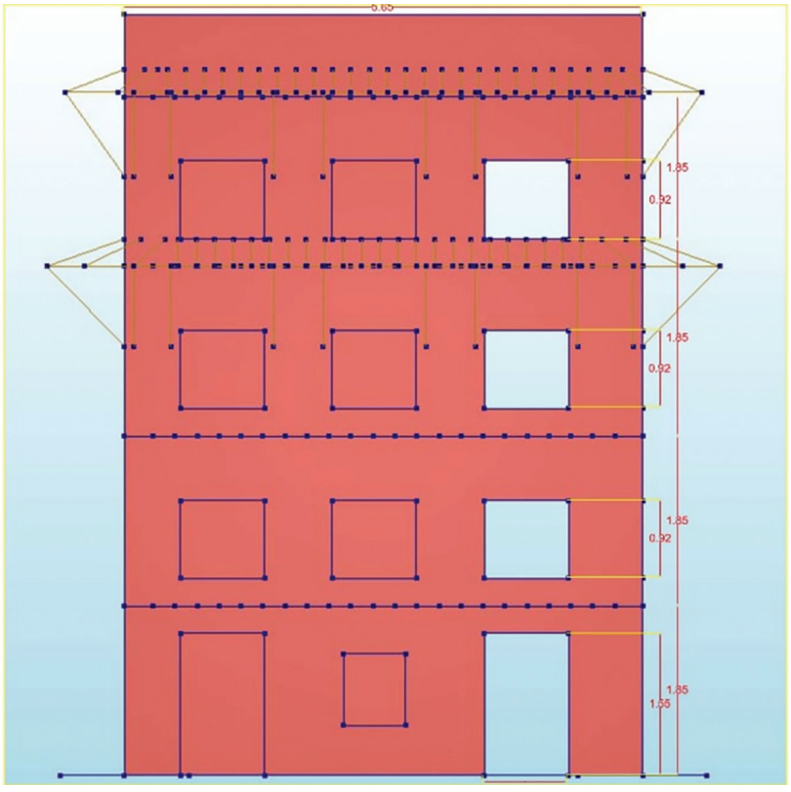

Figure 9: Back View

The traditional construction, the reliance on mud-mortar brick masonry, and the absence of internal load-bearing walls collectively suggest a high degree of susceptibility to shear failure and out-of-plane collapse during seismic events(Gautam & Rodrigues, 2021). The thinner wall construction on the top floor further compromises both stiffness and strength. The partial adjacency to a neighboring structure introduces complexities in accurately modeling dynamic interactions, as the effect of the shared wall whether beneficial or detrimental to seismic response is contingent upon the characteristics of the adjacent structure.

2.2 Material Property Characterization

2.2.1 Sample Collection

As an integral part of a broader initiative to document the building's construction system, observed damage patterns, and inherent dynamic features, brick samples were procured during the field survey conducted in December 2024. Adhering to established best practices for investigating heritage structures, which emphasize minimizing disruption to the building's fabric (Gautam et al., 2016)a total of six brick samples were meticulously extracted from discrete, unobtrusive sections of the building. These locations included integrity-hidden areas and portions of non-load-bearing walls. The original bricks were found to have consistent dimensions when measured directly, averaging approximately 22.5 cm in length, 11 cm in breadth, and 7.2 cm in thickness. These measurements provide precise, location-specific information regarding the building's original construction materials. Sampling points were carefully selected to be representative of the original building material, with a particular emphasis on the mud-mortar brick masonry walls, which constitute the primary load-bearing components. Areas that might possess historical significance, such as elaborate facades or physically prominent structural elements, were consciously avoided during sampling. The building's configuration, with three sides free-standing and one side abutting a neighboring structure, guided the selection of sampling sites to enable an assessment of potential differences in material exposure and condition. To analyze potential alterations due to reduced exposure, samples were taken from the free-standing sides where environmental degradation processes, such as weathering, could influence material qualities. Concurrently, at least one sample was obtained from the shared party wall. Due to constraints on sample size imposed by heritage conservation guidelines, the procured brick samples were subsequently cut into 40 mm × 40 mm × 40 mm cubes for laboratory testing, as illustrated in Figure 10.

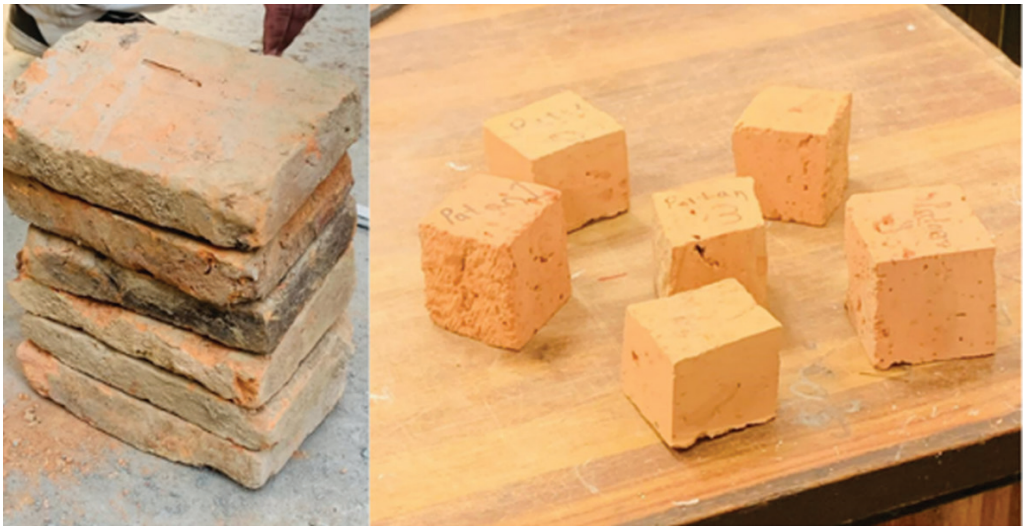

Figure 10: Original brick samples (left, stacked) and prepared 40 mm cube specimens (right) for uniaxial compressive strength testing.

2.2.2 Testing Procedure

To ensure both the dependability and international comparability of the findings, compressive strength tests were executed in strict accordance with ASTM C67 standards, which govern the testing of brick and structural clay tile(*Test Methods for Sampling and Testing Brick and Structural Clay Tile*, 2021). Utilizing a universal testing machine, the six 40 mm cubic specimens were subjected to uniaxial compressive testing. A consistent loading rate of 14 N/mm² per minute was applied to each specimen to induce a controlled failure within the allotted time. During the laboratory testing, each specimen was loaded progressively until failure occurred, and the maximum load sustained was meticulously recorded to facilitate the determination of its compressive strength. Three of the specimens were tested after being fully dried, while the remaining three were evaluated under ambient moisture conditions to represent the typical environmental exposure encountered in Patan. The mean results derived from these compressive strength tests are summarized in Table 5.

Table 5: Mean Compressive Strength of Brick Samples

Property Bricks	Test Specimen Size	Test Value (Mean)
Compressive Strength (Fully dried)	4cm × 4cm × 4cm	9.7 MPa
Compressive Strength (Ambient moisture)	4cm × 4cm × 4cm	11.2 MPa

Although not the most common approach, the utilization of 40 mm cubic specimens is an appropriate strategy for investigating historic buildings where the preservation of the structure and minimization of damage are of paramount importance. While smaller specimens may exhibit greater variability in results due to scale effects, research focused on historic masonry often favors smaller specimen sizes (typically in the range of 30-40 mm) to achieve a practical balance between the objectives of material characterization and heritage conservation(Lourenço et al., 2010). The measured compressive strengths (9.7 MPa for dry specimens, 11.2 MPa for ambient moisture specimens) are consistent with the established range of values for traditional bricks found in the Kathmandu Valley (which normally vary from 8 to 12 MPa when dry), where ambient conditions can often yield higher strength values due to the influence of moisture content(Gautam & Rodrigues, 2021). The applied loading rate of 14 N/mm² per minute falls comfortably within the 10 to 15 N/mm² per minute range specified by the ASTM C67 standard.

2.2.3 Limitations and Assumptions for Material Properties

According to research focused on Heritage Masonry, the use of 40 mm cubic specimens for testing may introduce scale effects, potentially leading to an increase in the variability of strength measurements when compared to tests conducted on full-size bricks (Lourenço et al., 2010). To mitigate this potential issue, the study verified the representativeness of the collected data by comparing it with published values for bricks found in Patan (Gautam & Rodrigues, 2021). A significant limitation in the material characterization process is the absence of mortar testing. This omission restricts the comprehensive assessment of the shear and tensile behavior of the masonry assemblage, properties essential for accurate seismic research and analysis. While timber parameters for elements such as floor diaphragms were based on published values for Sal wood, the properties of the mortar were derived from regional studies, assuming a shear strength in the range of 0.1-0.3 MPa (Adhikari et al., 2025). To facilitate future validation efforts with more extensive testing, these assumptions regarding material properties are openly documented within this study.

2.3 Numerical Modeling and Analysis

A three-dimensional (3D) finite element model of the case study building was developed utilizing DIANA FEA 10.5 software, predicated on the assumption of homogenized wall masonry characteristics.

2.3.1 Model Development

The structural masonry walls within the model were represented using thin shell elements, which were constrained with fixed boundary conditions at the plinth level. For the execution of pushover studies, macro-element methodologies were employed, primarily due to their relative ease of implementation and their reduced computational demands. Similarly, isometric area components were utilized for the discretization process during analysis. These components are advantageous as they can accurately discretize and represent geometrically complex structures in computational modeling. For finite element analysis to yield reliable and consistent findings, the use of elements that retain identical areas and shapes irrespective of their orientation is essential. The capacity of isometric area components to effectively manage irregular geometries and variable load circumstances, thereby ensuring accurate predictions of stress-strain distribution and deformation, justifies their adoption. Owing to its critical importance for achieving accuracy in structural analysis, particularly when evaluating performance and stability under varying loading conditions, isometric area components form a fundamental building block of sophisticated engineering simulations. The completed model was composed of 2995 nodes. Horizontal cross timber beams were incorporated at the lintel (*dalin*) locations, with the cross-section of these beams defined as 150 mm × 150 mm. The roof structure of each tier was modeled to include timber rafters, joists, and beams. For defining the failure criteria of the brick masonry, the rotating total-strain-crack model, originally proposed by (Vecchio et al., 1986) was adopted. This model was selected because it is less sensitive to mesh orientation, performs better when analyzing complex stress states, and helps to avoid the phenomenon of stress locking.

2.3.2 Adopted Material Parameters for Modeling

For the numerical model, material properties representing the in-situ brick with mud mortar construction were required. However, a comprehensive set of validated numerical parameters for traditional Nepalese mud mortar masonry is not readily available in the literature. Therefore, as a necessary and documented approximation, parameters for a similar traditional material, lime-surkhi masonry, were adapted from studies by (Endo & Hanazato, 2020) and (Bashyal et al., 2024), with additional reference to (Motra et al., 2021) and NZSEE guidelines. To anchor the model with site-specific data, the experimentally determined compressive strength of 9.7 MPa (Table 5) was directly inputted as the primary compressive strength value (fc). In alignment with the data adopted by Endo for uniaxial behavior, a linear softening curve was assumed for the material in tension, while a parabolic curve was utilized for its response in compression. For the brick masonry, the critical crack strain was considered 0.0005. Similarly, the fracture energy was taken as 13.5 N/m in tension and 2,700 N/m in compression, consistent with the values adopted by Endo & Hanazato, 2020. The key adopted material parameters are summarized in Table 6.

Table 6: Summary of Adopted Material Parameters for Lime Surkhi Masonry, primarily based on (Bashyal et al., 2024; Endo & Hanazato, 2020; Motra et al., 2021)

Parameter	Value	Unit	Source/Note
Young's Modulus Ex, Ey	1358	MPa	(Bashyal et al., 2024)
Shear Modulus Gxy	543.2	MPa	(Bashyal et al., 2024)
Mass density ρ	19.6	kg/m ^{3}	(Bashyal et al., 2024)
Bed joint tensile strength ft	0.15	MPa	(Bashyal et al., 2024)
Fracture energy in tension GfI	13.5	N/m	(Endo & Hanazato, 2020)
Compressive strength fc	9.7	MPa	Test (This study)
Fracture energy in compression Gc	2700	N/m	(Endo & Hanazato, 2020)
Angle between diagonal crack and bed joint α	0.785	rad	(Bashyal et al., 2024)
Factor to strain at compressive strength εc, fac	4	-	(Bashyal et al., 2024)
Friction angle φ	0.4	rad	(Bashyal et al., 2024)
Cohesion C	0.2	MPa	(Bashyal et al., 2024)
Fracture energy shear Gsh	20	N/m	(Bashyal et al., 2024)
Critical Crack Strain (Tension)	0.0005	-	(Endo & Hanazato, 2020)

2.4 Pushover Analysis Procedure

To evaluate the structure's seismic behavior using the DIANA software, a pushover analysis was systematically conducted. This process encompassed the creation of a detailed 3D model, the assignment of appropriate material properties, the definition of applied loads, and the meshing of the model. An eigenvalue analysis was initially performed to identify the structure's natural vibration modes. This was followed by a nonlinear analysis designed to track the deformation of the structure under the incrementally applied pushover load. Finally, a pushover curve was developed by plotting the total base shear against the corresponding horizontal displacement at a control point, thereby revealing the structure's capacity to withstand lateral seismic forces. The foundation's boundary condition was considered rigid, and the applied load's boundary condition included the structure's self-weight. Similarly, a pushover analysis was executed in both the X and Y principal directions. The lateral load applied incrementally in these directions corresponded to an initial value of 0.05g for the analysis steps.

2.5 Fragility Curve Development

To assess a symmetric, G+4 story masonry building where the first two modes were identified as pure translational movements, the nonlinear pushover capacity curve was transformed into a format suitable for standardized seismic assessment. The capacity curve was idealized as an equivalent bilinear representation, adhering to the principle of equal energy up to the ultimate displacement, as outlined in ATC-40 and FEMA 356 (ATC-40, 1996; FEMA 356, 2000). Given the building's symmetry and the dominance of the first mode, this simplification effectively captures the essential lateral-force behavior while defining two key performance parameters associated with the first translational mode: the yield roof displacement (Δy) and the ultimate roof displacement (Δu). These parameters signify the onset of significant inelasticity and the deformation limit, respectively, and thereby form the basis for the subsequent delineation of damage states. To express these parameters in spectral coordinates for the purpose of fragility modeling,

each displacement value was converted using the first-mode participation factor (Γ_1) and the first-mode roof amplitude (ϕ *roof*), which were obtained from the DIANA FEA. According to the equation:

$$S_d = \frac{\Delta}{\Gamma_1 \times \phi_{roof}} \quad \ldots\ldots (1)$$

Using this relationship, the spectral displacement at yield ($S_{d,y}$) and the spectral displacement at the ultimate state ($S_{d,u}$) were obtained.

Damage thresholds for a masonry structure were defined in accordance with the recommendations of (Barbat et al., 2008) employing the following median spectral displacements:

- Slight Damage (DS_1): $S_{d,1} = 0.7 \times S_{d,y}$
- Moderate Damage (DS_2): $S_{d,2} = S_{d,y}$
- Extensive Damage (DS_3): $S_{d,3} = S_{d,y} + 0.25 \times (S_{d,u} - S_{d,y})$
- Complete Collapse (DS_4): $S_{d,4} = S_{d,u}$

A uniform lognormal standard deviation (β), as recommended by HAZUS guidelines, was applied consistently across all defined limit states. Each fragility curve, representing the conditional probability of reaching or exceeding a damage state 'j' given a spectral displacement S_d, was expressed using the lognormal cumulative distribution function:

$$P\,[DS \geq j \mid S_d] = \Phi\left[\frac{ln(S_d) - ln(S_{d,median,j})}{\beta}\right] \quad \ldots\ldots\ldots (2)$$

where Φ denotes the standard normal cumulative distribution function, and $S_{d,median,j}$ represents the median spectral displacement for damage state 'j'. This formulation facilitates a probabilistic evaluation of seismic performance and supports the development of informed risk mitigation strategies.

2.6 Performance Assessment using Capacity Spectrum Method (CSM)

The critical comparison between the structure's inherent seismic capacity and the anticipated seismic demand was conducted utilizing the CSM), a robust graphical procedure widely employed in performance-based earthquake engineering (ATC-40, 1996). This method operates within the Acceleration-Displacement Response Spectrum (ADRS) domain, necessitating the transformation of the Multi-Degree-of-Freedom (MDOF) structure's pushover curve (which plots base shear, V_{base}, versus roof displacement, Δ_{roof}) into an equivalent Single-Degree-of-Freedom (SDOF) capacity spectrum (plotting S_a versus S_d). This conversion leverages the dynamic properties of the structure's dominant mode in the direction of analysis, specifically the modal participation factor (PF_1 or Γ_1), the modal amplitude at the control node ($\phi_{roof,1}$), and the effective modal mass (M_1*). The resulting capacity spectrum is conceptually illustrated in Figures 14–19 (representing capacity curves). Concurrently, the seismic hazard is represented by appropriately scaled, 5%-damped elastic response spectra (also presented in ADRS format) that reflect target earthquake intensities (PGA levels). The CSM fundamentally resolves to find the Performance Point (PP), defined by the coordinates ($S_{d,PP}$, Sa_pp). It represents the structure's expected maximum response under the given seismic hazard. This is achieved through an iterative process that seeks the intersection of the capacity spectrum and the demand spectrum. The latter is systematically reduced to account for the beneficial effects of increased effective damping (β_{eff}) arising from hysteretic energy dissipation as the structure responds inelastically. The iterative procedure refines estimates of the effective period (T_{eff}) and effective damping (β_{eff}) at trial displacement points along the capacity curve, adjusting the demand spectrum via spectral reduction factors until convergence is achieved,

thereby satisfying the equilibrium between capacity and demand while considering inelastic behavior. The location of this converged Performance Point, relative to the previously defined damage state thresholds, provides a direct, quantitative assessment of the anticipated structural performance level for each analyzed seismic hazard scenario.

The seismic demand for the structural analysis was characterized using response spectra developed in the ADRS format, which plots normalized spectral acceleration (Sa/g) against spectral displacement (S_d). These demand spectra were constructed following the procedures specified in the Nepal National Building Code (NBC 105, 2020). The process commenced with defining the elastic response spectrum shape based on site-specific soil conditions. For this study, Soil Type D was considered. The spectral shape factor, Ch(T), as a function of the natural period (T), was determined using NBC 105 Figure 4-2 and the associated Equation 4.1(2). The parameters defining the shape for Soil Type D were sourced from NBC 105 Table 4-1: the upper period of the constant acceleration plateau, Tc = 2.0 s; the peak spectral acceleration amplification factor, α = 2.25; and the coefficient controlling the descending branch, K = 0.8. As the analysis corresponds to the Equivalent Static Method, the lower period of the constant acceleration plateau, Ta, was taken as 0 seconds, as indicated by Note 1 in Table 4-1 of the code. Based on these parameters, Ch(T) was calculated as:

$$Ch(T) = \alpha = 2.25, \text{ for } 0\ s \le T \le 2.0\ s$$

$$Ch(T) = \alpha\ [\ K + (1-K)\ (Tc/T)^{2}] = 2.25\ [\ 0.8 + (1-0.8)\ (2.0/T)^{2}], \text{ for } 2.0\ s < T \le 6.0\ s \quad \text{.....(3)}$$

The normalized elastic spectral acceleration (Sa/g) for 5% damping was then computed for a range of periods (T) using the fundamental relationship provided in NBC 105:

$$Sa/g = Z \times I \times Ch(T) \quad \text{.....(4)}$$

Where Z is the seismic zone factor, representing the Peak Ground Acceleration (PGA) for the specific hazard level being considered, and I is the importance factor of the structure. For this investigation, a crucial factor (I) of 1.0 was adopted. To evaluate the structural performance under varying seismic intensities, demand spectra were generated for four distinct PGA levels (Z values): 0.0915g, 0.15g, 0.164g, and 0.18g (and higher, as analysis progressed). Finally, to convert the spectra from the Sa/g vs. T format to the required ADRS format (Sa/g vs. S_d), the spectral displacement (S_d) corresponding to each period (T) and Sa/g value was calculated using the standard relationship:

$$S\_d = S\_a \times (T^2 / (4\pi^2)) = (Sa/g) \times g \times (T^2 / (4\pi^2)) \quad \text{..... (5)}$$

Where g is the acceleration due to gravity (9.81 m/s²). The resulting pairs of (S_d ,Sa/g) for each of the four specified PGA levels were then plotted to establish the seismic demand curves used in the capacity spectrum assessment.

3. Results and Discussion

3.1 Dynamic Characteristics

An eigenvalue analysis was executed to ascertain the inherent dynamic properties that govern the building's linear elastic response. The computed natural frequencies (or periods) and their associated mode shapes are pivotal for understanding the structure's susceptibility to dynamic loading and for subsequent response spectrum analysis. Key results of the first five modes of vibration are summarized in Table 7.

Table 7: Modal Properties of the Studied Building

Mode No.	Period (s)	Frequency (Hz)	X-dir Mass Participation (%)	Y-dir Mass Participation (%)	Cumulative X-dir Mass (%)	Cumulative Y-dir Mass (%)
1	0.594	1.684	84.50	0.05	84.50	0.05
2	0.388	2.576	0.10	87.20	84.60	87.25
3	0.279	3.589	2.30	0.02	86.90	87.27
4	0.185	5.405	0.01	5.45	86.91	92.72
5	0.155	6.451	5.15	0.00	92.06	92.72

The fundamental period of the structure, corresponding to Mode 1, is T_1 = 0.594 s. This mode primarily activates a translational response in the X-direction, engaging 84.5% of the effective mass. The second mode, with a period T_2 = 0.388 s, is translational in the Y-direction, mobilizing 87.2% of the mass in that axis and thereby increasing the cumulative Y-direction mass participation to 87.25%, while the cumulative X-direction mass participation remains approximately 84.6%. In total, over 90% of the mass is activated in both principal directions within the first five modes (92.06% in the X-direction and 92.72% in the Y-direction). This confirms that these fundamental modes adequately capture the dominant dynamic behavior of the structure, justifying the use of analysis procedures, such as pushover analysis, that are based on these modes. The proximity of the third modal frequency (3.589 Hz) to the second (2.576 Hz), coupled with some X-direction mass participation (2.30%) in the third mode, might suggest a minor degree of torsional coupling; however, its overall contribution to the response appears to be limited. Figure 11 presents a visual comparison between the observed cracking pattern on the actual building and the damage predicted by the numerical model.

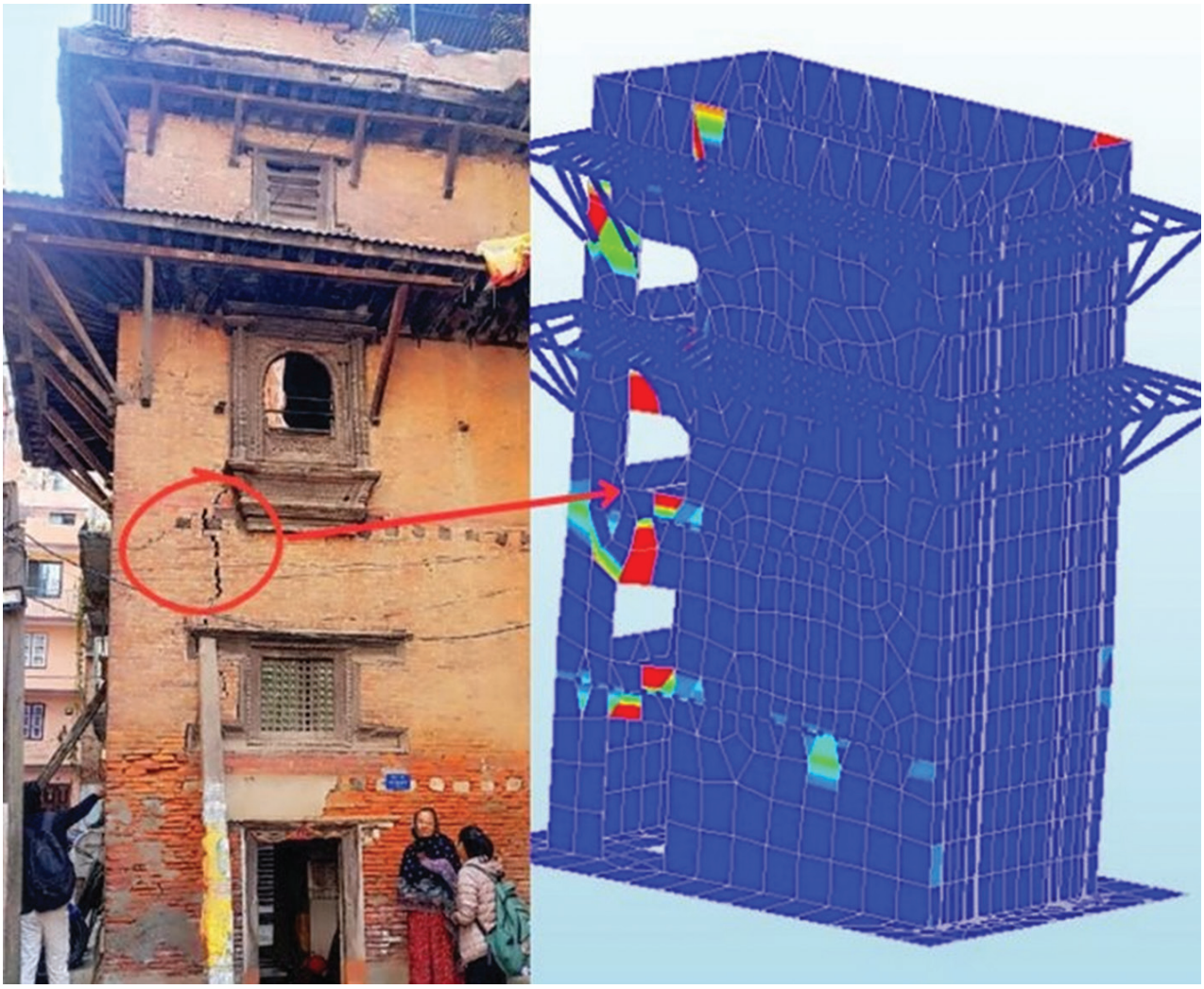

Figure 11: Observed cracking pattern and predicted damage from FE analysis.

3.2 Nonlinear Static (Pushover) Analysis

To investigate the building's inelastic behavior, potential for strength degradation, and ultimate deformation capacity, a nonlinear static pushover analysis was executed. This involved applying a predefined lateral load pattern (in this case, proportional to the first mode shape) incrementally until either structural failure was indicated or a target displacement was achieved. DIANA FEA 10.5 was used to perform the analysis. Damage accumulation over time was simulated using nonlinear material models for masonry, which could capture crushing and cracking behavior.

- **X-Direction Response:** The maximum base shear ($V_{b,max}$,*X*) was determined to be 410.14 kN. This peak resistance corresponded to an ultimate roof displacement (du,X) of 36.49 mm and was associated with a lateral load factor equivalent to 0.727g.
- **Y-Direction Response:** In the Y-direction, the maximum base shear ($V_{b,max}$,*Y*) was found to be 236.46 kN, occurring at an ultimate roof displacement (du,Y) of 65.54 mm. This peak resistance corresponded to a load factor of 0.447g.

The pushover curve depicting the nonlinear capacity in the Y-direction is shown in Figure 12. The curve for the X-direction exhibits a similar general shape but with different characteristic values, as presented later in Figure 14, which includes its bilinear idealization.

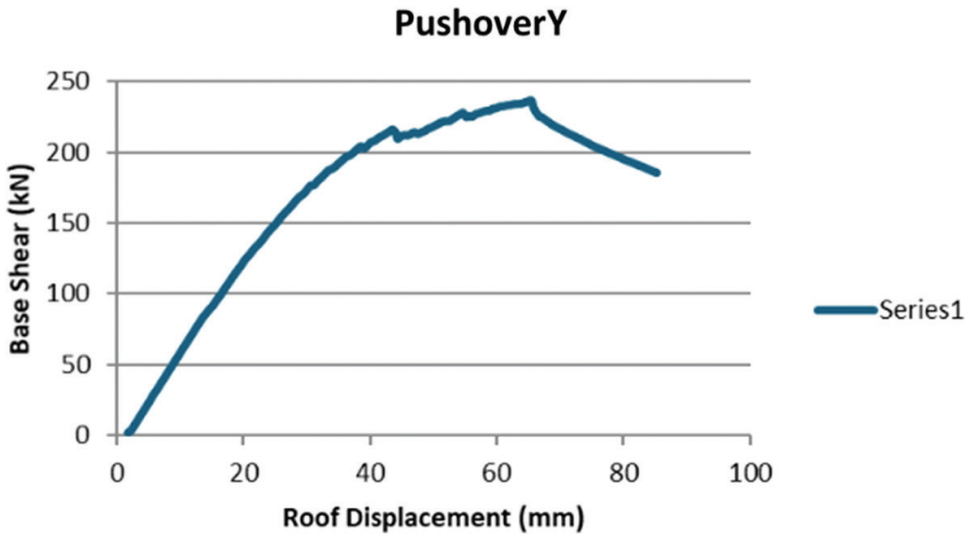

Figure 12: Nonlinear capacity curve for the Y-direction.

The significant discrepancy in both the peak base shear (capacity) and the ultimate displacement observed between the X and Y directions clearly highlights the anisotropic nature of the building's seismic response. This anisotropy stems from the building's specific geometric configuration (a rectangular plan with dimensions of 5.65m in X versus 2.52m in Y), its structural layout (including the orientation of walls and the distribution of openings), and potentially the specific lateral load pattern applied. The finding that the Y-direction exhibits lower capacity, but greater ductility (in terms of displacement) compared to the X-direction is a critical outcome for a comprehensive seismic evaluation. For the subsequent stages of defining damage states and performance points, the results from the X-direction analysis (which showed higher strength but lower ultimate displacement) were primarily used, as this often represents a critical case for assessing certain damage thresholds, although the Y-direction behavior must also be considered in a full assessment.

3.3 Definition of Performance Levels and Damage States

Based on the characteristic displacements (yield displacement, $D_y \approx 14.16$ mm, and ultimate displacement, $d_u = 36.49$ mm, as identified from the X-direction capacity curve shown in Figure 14), distinct performance levels corresponding to predefined damage states were quantified. This was accomplished using the framework proposed by(Lagomarsino & Giovinazzi, 2006), adapted for roof displacements (Δ_{roof}). The adopted definitions and their corresponding calculated roof displacements for the analyzed building are presented in Table 8.

Table 8: Performance Levels and Corresponding Roof Displacements (Δ_{roof}) for the X-Direction

Performance Level / Damage Extent	Defining Equation	Calculated Δ_{roof} (mm)
IO / Slight (DS1)	0.7Sdy	9.912
LS / Moderate (DS2)	Sdy	21.24
CP / Extensive (DS3)	Sdy + 0.25 * (Sdu – Sdy)	25.325
Collapse (DS4)	Sdu	36.49

3.4 Fragility Analysis

To introduce a probabilistic perspective to the assessment of seismic performance and to account for inherent uncertainties in material properties, modeling assumptions, and seismic demand characterization, fragility curves were developed. These curves express the conditional probability of reaching or exceeding predefined damage states (DSi) as a function of an engineering demand parameter (EDP), such as roof displacement (Δ_{roof}). Figure 13 presents the fragility curves derived for the masonry building, plotting the probability of exceedance against roof displacement. Each curve corresponds to one of the four damage states defined previously (Slight/IO, Moderate/LS, Extensive/CP, Collapse).

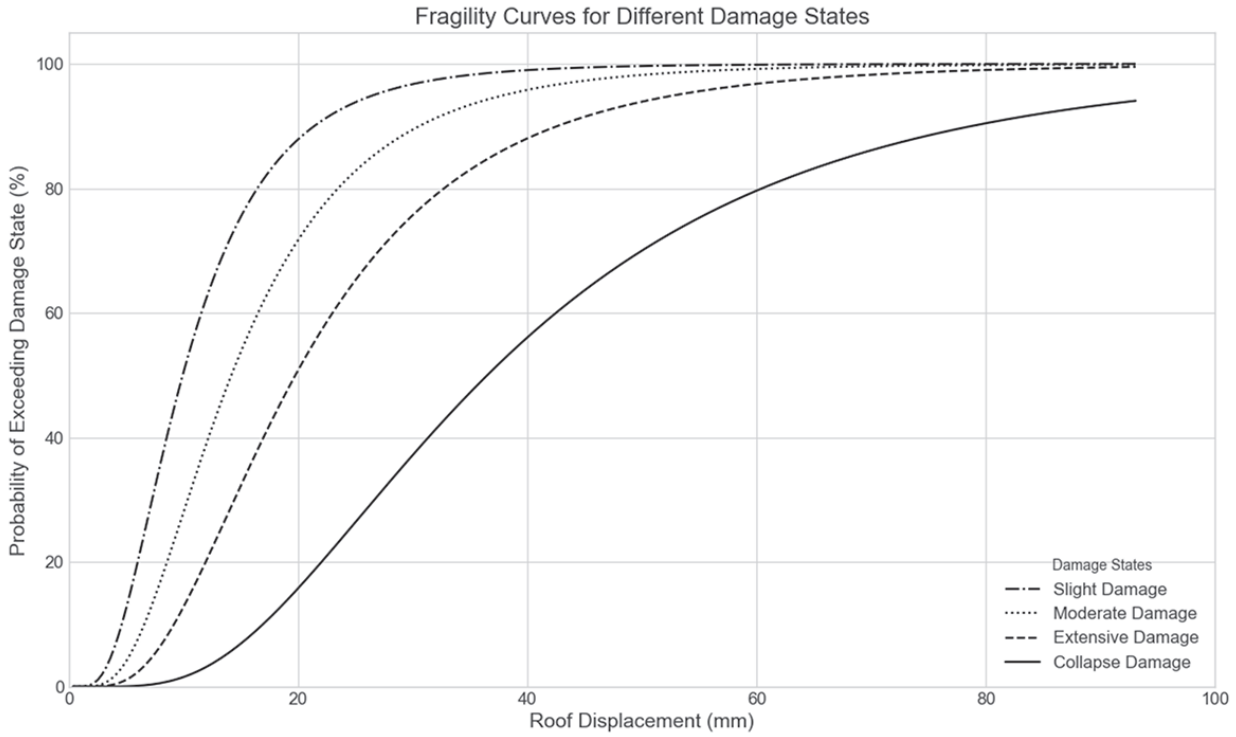

Figure 13: Fragility curves, probability of exceedance vs roof displacement (Δ_{roof}).

Interpretation of Fragility Curves:

- **Curve Identification:** Based on the displacement thresholds presented in Table 6, the curves represent the following:
  - Dash-Dot Curve: DS1 (Slight/IO) - Median displacement around 10-12 mm.
  - Dotted Curve: DS2 (Moderate/LS) - Median displacement around 20-23 mm.
  - Dashed Curve: DS3 (Extensive/CP) - Median displacement around 25-28 mm.
  - Solid Curve: DS4 (Collapse) - Median displacement around 40-50 mm.

(It is noted that the median displacement for collapse derived from the curve appears higher than the deterministic ultimate displacement, du, of 36.5 mm obtained from the X-direction pushover analysis. This difference could arise from the statistical methodology employed for fragility derivation, the inclusion of various uncertainties, or potentially the curve representing an averaged or combined directional behavior, or the fitting process of the lognormal distribution.)

- **Probabilistic Performance:** The curves quantify the likelihood of experiencing various levels of damage. For instance, at a roof displacement of 20 mm:
  - There is an extremely high probability (~98%) of experiencing at least Slight damage (DS1).
  - There is a high probability (~85%) of experiencing at least Moderate damage (DS2).
  - There is a significant probability (~40-50%) of experiencing at least Extensive damage (DS3).
  - There is a lower probability (~10-15%) of reaching or exceeding the Collapse state (DS4).
- **Uncertainty Representation:** The slope of the fragility curves reflects the uncertainty associated with predicting the onset of a particular damage state. Steeper slopes (e.g., for DS1 and DS2) indicate lower dispersion and, consequently, higher confidence in the damage state occurring around the median displacement value. The gentler slope observed for DS4 suggests greater variability or uncertainty in predicting collapse based solely on roof displacement.
- **Damage Progression:** The spacing between the curves visually illustrates the range of displacements over which the various levels of damage are expected to manifest as the deformation demand increases.

3.5 Seismic Demand and Performance Point Evaluation (CSM)

To contextualize the probabilistic data from the fragility analysis, the building's performance was deterministically assessed against code-specified seismic demands using the Capacity Spectrum Method (CSM). The seismic performance of the representative unreinforced masonry (URM) building was assessed using the Capacity Spectrum Method (CSM) as described in (ATC-40, 1996).This method involves transforming both the structural capacity curve (obtained through nonlinear pushover analysis) and the seismic demand curve into the ADRS format, which allows for a direct comparison of the structure's capacity against the seismic demand. The pushover curve, which provides the relationship between base shear (V_{base}) and roof displacement (Δ_{roof}) for the X-direction, was converted into the ADRS format to represent an equivalent Single-Degree-of-Freedom (SDOF) system. The modal parameters required for this transformation (Γ_1, $\phi_{roof,1}$), W, α_1) were derived from the FE model analysis for the first mode in the X-direction, using the standard equations:

$$\Gamma_1 = (\Sigma (w_i \times \phi_{i,1})) / (\Sigma (w_i \times \phi_{i,1}^2)) \quad \text{.....} \quad (6)$$

$$\alpha_1 = ((\Sigma (w_i \times \phi_{i,1}))^2) / (W \times \Sigma (w_i \times \phi_{i,1}^2)) \quad \text{.....} \quad (7)$$

where w_i represents the seismic weight at floor i, $\phi_{i,1}$ is the amplitude of the first mode shape at floor i, and W is the total effective seismic weight of the structure.

The elastic seismic demand was defined using the 5% damped acceleration response spectrum provided by NBC 105:2020 for Soil Type D, with an Importance Factor (I) set to 1.0. Demand spectra were generated for various Peak Ground Acceleration (PGA) values. Figure 14 illustrates the bilinear idealization of the X-direction pushover curve, with the indicated damage state thresholds.

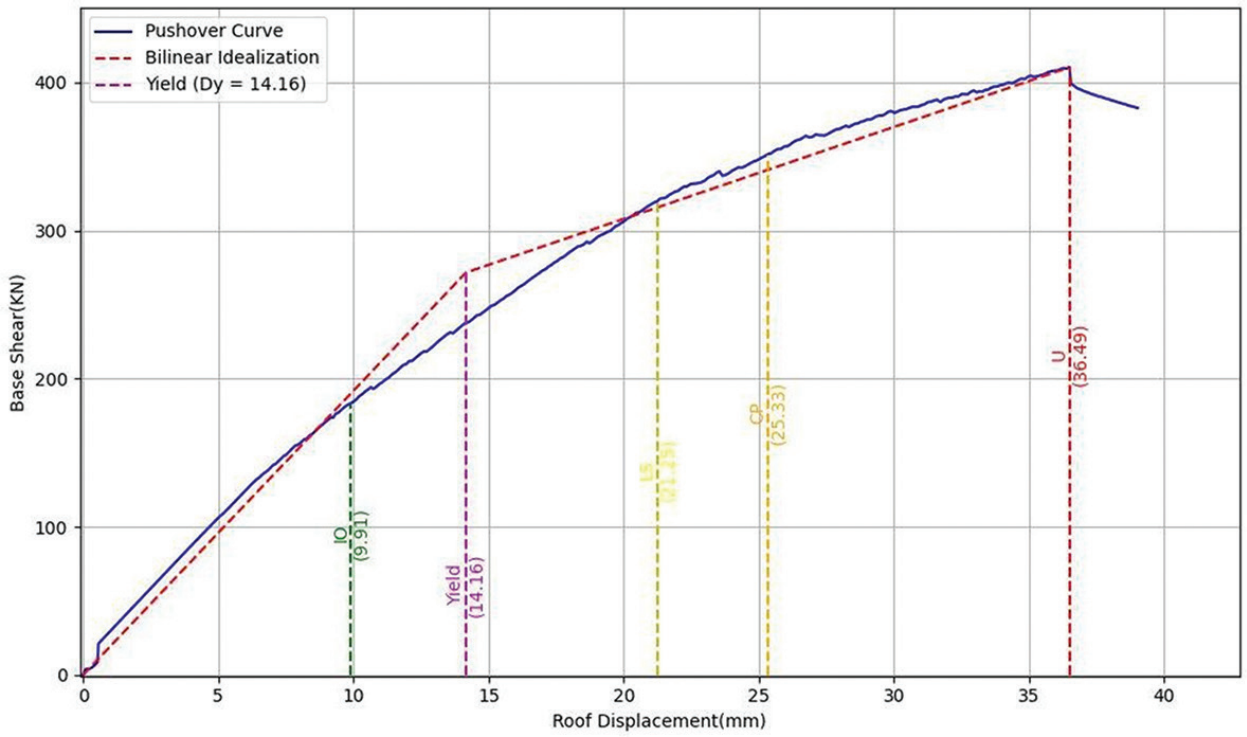

Figure 14: Bilinear idealization of the X-direction pushover curve

Table 9 summarizes the spectral displacements (S_d) at the performance point for the various PGA values considered, focusing on the X-direction response.

Table 9: Performance Point (S_d) for Various PGA Levels (X-Direction)

PGA (Z value)	Performance Point S_d (mm)	Corresponding Approx. Δ_{roof} (mm) (Assuming $\Gamma_1 \phi_{roof,1} \approx 1.3$)	Inferred Damage State (from Table 8 and Figure 14)
0.0915g	27.58	35.85	Approaching Collapse (DS4)
0.15g	52.11	67.74	Exceeds Collapse (DS4)
0.164g	59.13	76.87	Exceeds Collapse (DS4)
0.18g	70.48	91.62	Exceeds Collapse (DS4)
0.21g	101.54	132.00	Exceeds Collapse (DS4)
0.211g	Does not exist	-	Instability/Collapse

The Capacity-Demand curves for the different PGA levels are shown in Figures 14-19 below.

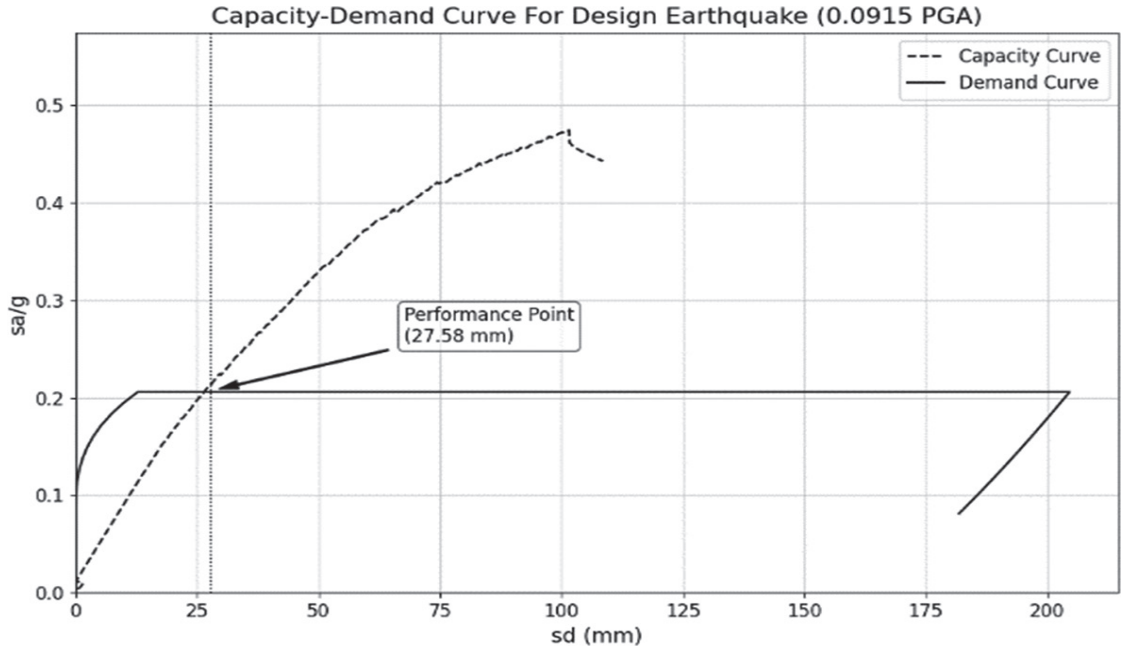

Figure 15: Capacity vs Demand curves for PGA 0.0915g

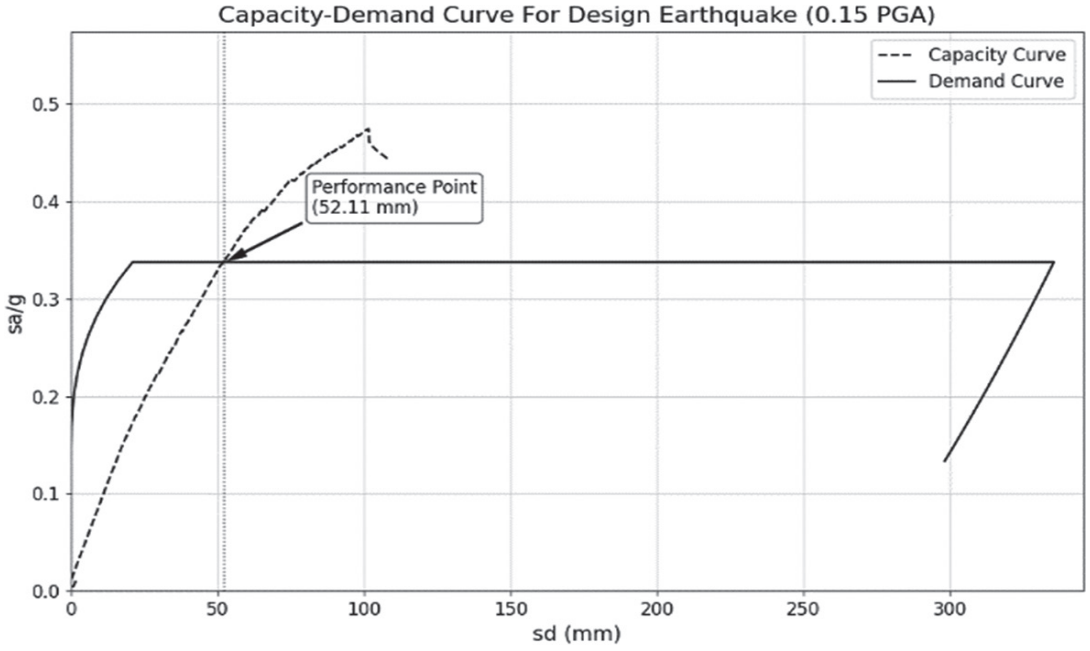

Figure 16: Capacity vs Demand curves for PGA 0.15g

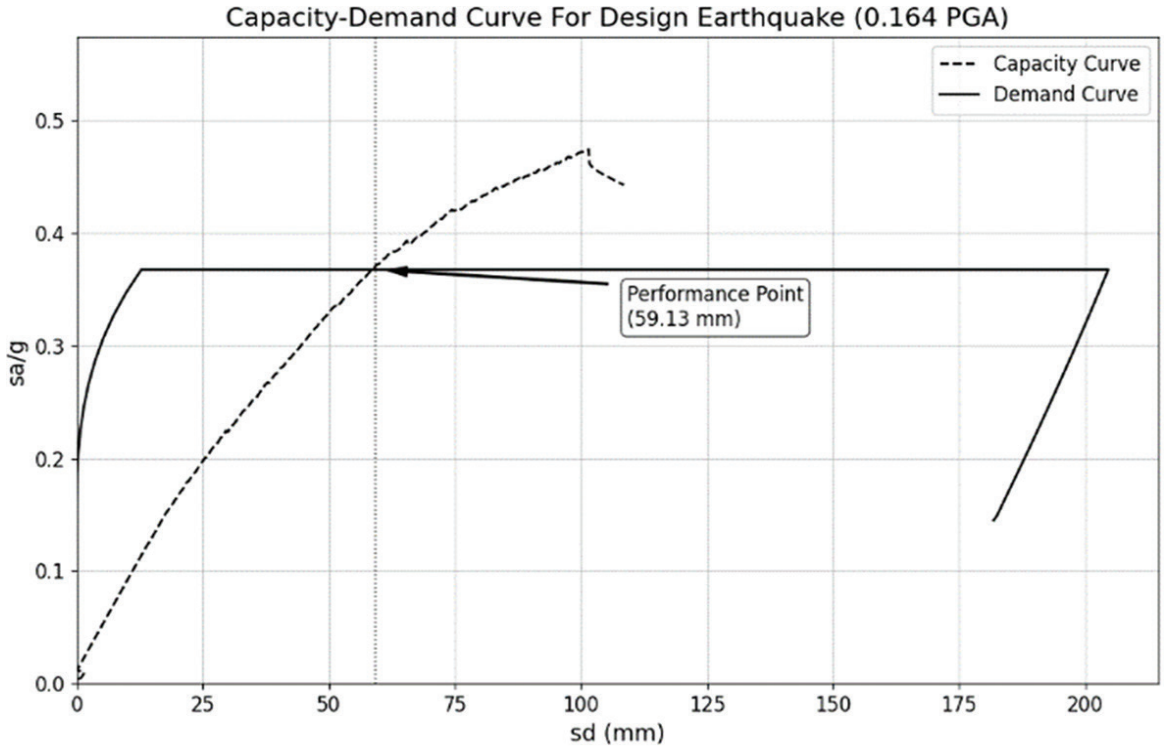

Figure 17: Capacity vs Demand curves for PGA 0.164g

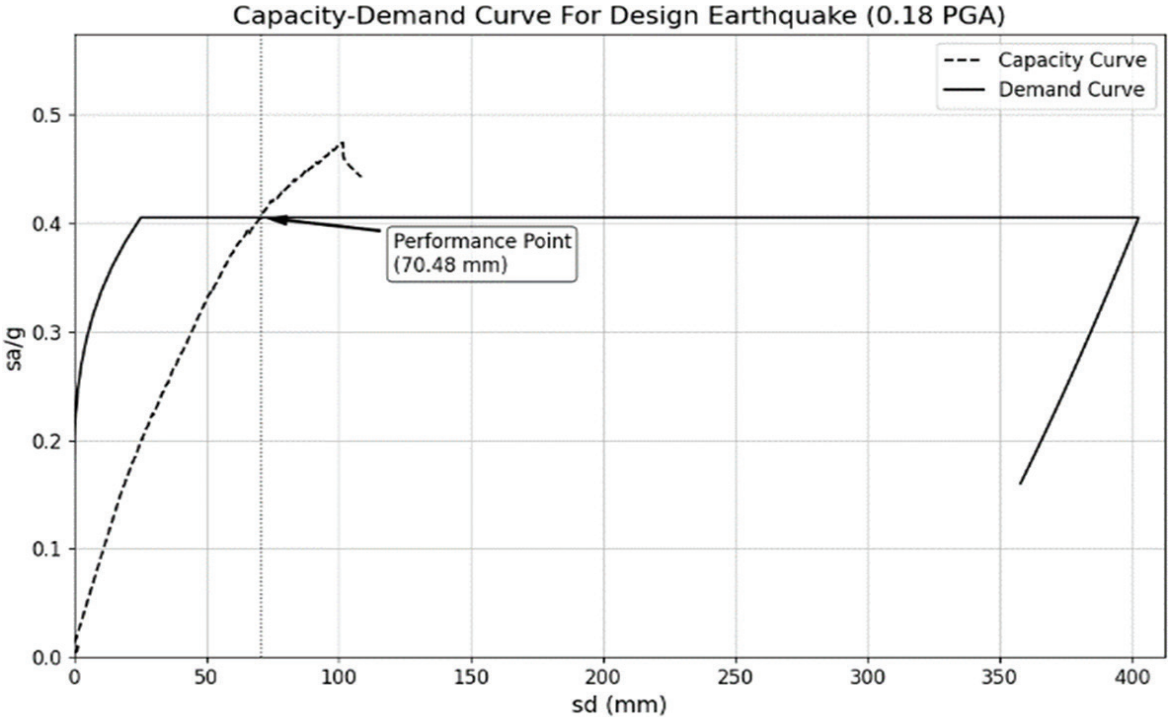

Figure 18: Capacity vs Demand curves for PGA 0.18g

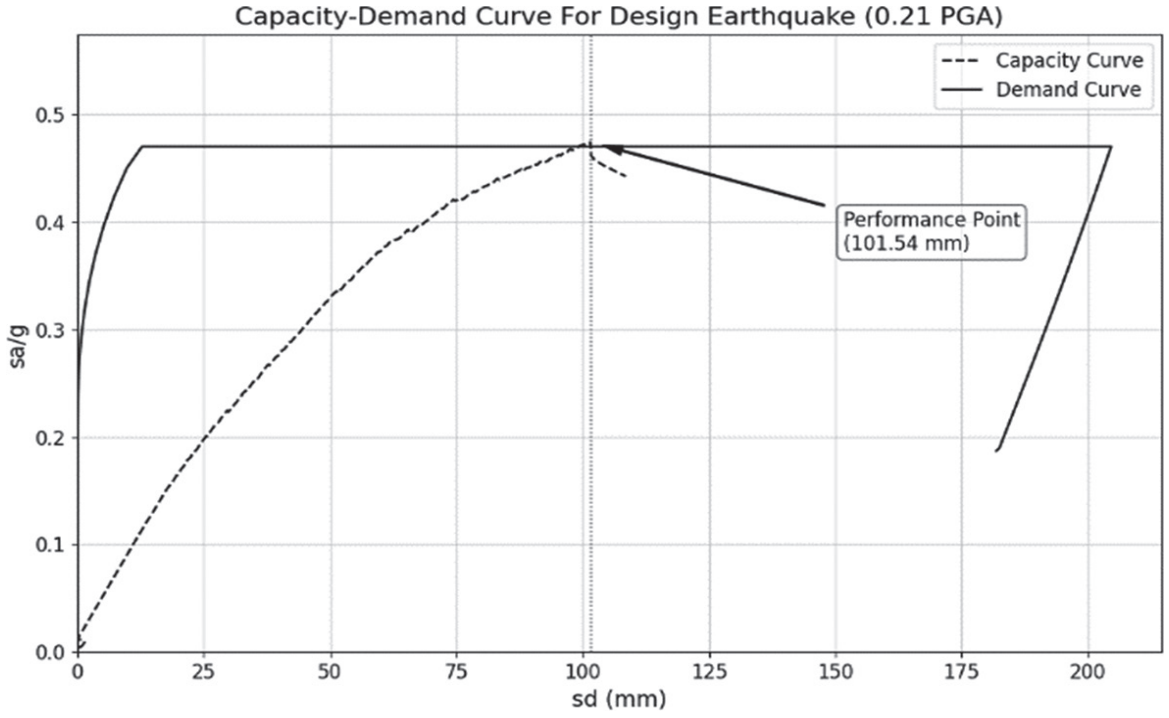

Figure 19: Capacity vs Demand curves for PGA 0.21g.

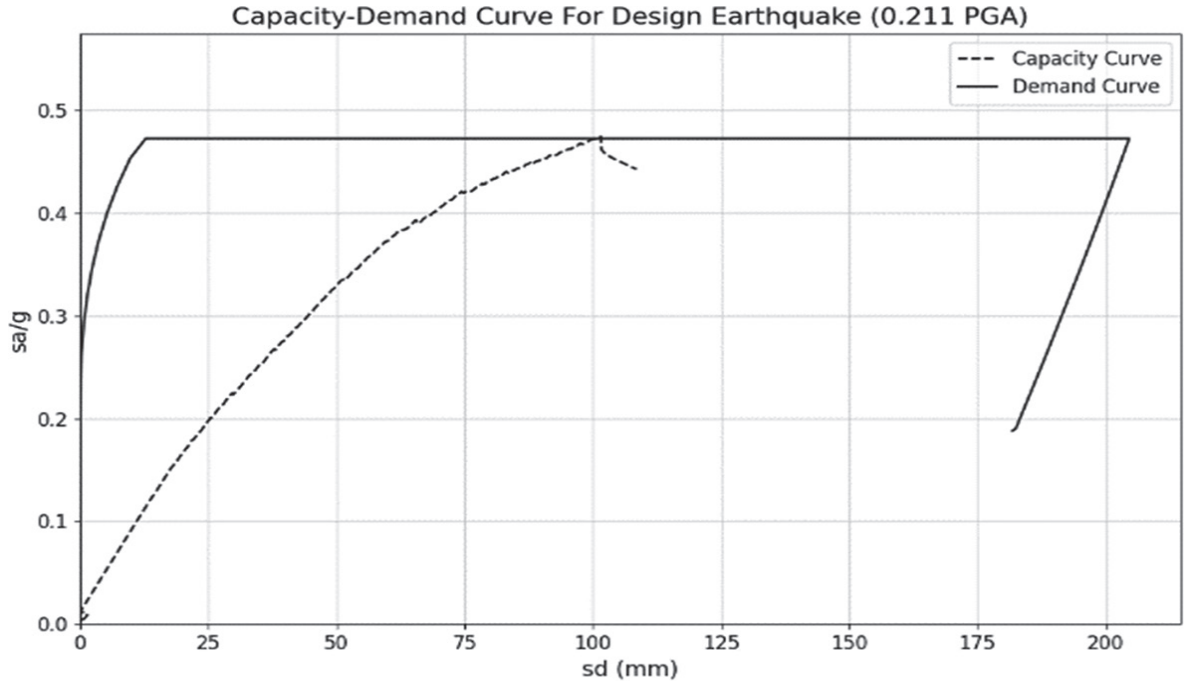

Figure 20: Capacity vs Demand curves for PGA 0.211g

3.6 Discussion of Seismic Performance

The eigenvalue analysis successfully established the fundamental dynamic identity of the structure, confirming the dominance of the first few modes, which is typical for low-to-medium rise buildings. The pushover analysis provided the essential capacity curve, quantifying the building's resistance as it transitions through elastic and inelastic ranges. The defined performance levels as shown in Table 8 translate these capacities into expected damage thresholds. A critical aspect of this assessment is the comparison of the predicted seismic demand with the capacity thresholds. A direct comparison requires converting the spectral displacement (S_d) from the performance point back to the roof displacement (Δ_{roof}) using the relation $\Delta_{roof} = \mathbf{\Gamma_1}_{roof,1} S_d$ With these it was found that at a PGA of 0.0915g, the S_d is 27.525 mm. Similarly, at higher PGAs, the calculated S_d values were found to be large. It was found the roof displacements exceeding the ultimate capacity of du=36.49 mm indicated structural collapse. The analysis also revealed that a performance point did not exist for a PGA of 0.211g. This implies that at this level of seismic demand, the structure becomes unstable and collapses before the seismic energy input, as the capacity and demand spectra do not intersect.

Collectively, these results, derived from the DIANA FEA 10.5 analysis, suggest a high seismic vulnerability for the studied masonry building when subjected to the NBC 105:2020 seismic hazard for soil type D. The structure is predicted to experience displacements exceeding Collapse Prevention limits and reaching or exceeding Collapse limits even under moderate seismic intensities (PGA ≈ 0.1g). This level of performance is often characteristic of older, unreinforced masonry structures that were not designed according to modern seismic codes. The analysis underscores a significant risk and highlights the potential need for seismic retrofitting to achieve acceptable performance levels, particularly Life Safety or Immediate Occupancy, under design-level earthquakes. The limitations of this study include those inherent in pushover analysis (e.g., reliance on assumed load patterns, potential neglect of higher mode effects, uncertainties in material modeling) and the Capacity Spectrum Method. Furthermore, the analysis primarily represents the building's response pseudo-3D; a full 3D analysis incorporating bidirectional loading and torsion might reveal additional vulnerabilities. Future work could involve nonlinear time history analysis for a more definitive assessment and exploring the efficacy of potential retrofitting interventions.

4. Conclusions

This study presented a comprehensive seismic vulnerability assessment of a representative traditional unreinforced masonry building located in Patan, Nepal, a region characterized by high seismicity and invaluable cultural heritage. Patan, a UNESCO World Heritage Site in the Kathmandu Valley, exhibits acute vulnerability due to its dense settlement, aging structures, and narrow lanes that hinder emergency response during disasters (Upreti & Yoshida, 2009). Motivated by the demonstrated vulnerability of such structures in past earthquakes and the limitations of existing generic models, this research aimed to develop specific fragility functions and capacity parameters that reflect local construction practices. Through detailed field investigations, material testing (specifically, brick compressive strength), and advanced numerical modeling using DIANA FEA 10.5, the following key findings were obtained:

1. **Dynamic Characteristics:** The fundamental translational periods of the structure were identified as T_1 = 0.594 s and T_2 = 0.388 s. With over 90% mass participation within the first three modes, the suitability of employing pushover analysis for this type of structure was confirmed.
2. **Nonlinear Capacity:** Pushover analyses revealed significant directional anisotropy in the building's response. The structure exhibited higher strength but a lower ultimate displacement capacity in its X-direction ($V_{b,max}$, ,X = 410 kN, d_u,X = 36.5 mm) when compared to its Y-direction ($V_{b,max}$,Y = 236 kN, d_u,Y = 65.5 mm).

3. **Probabilistic Fragility:** Fragility curves, linking roof displacement to the probability of exceeding Immediate Occupancy (IO), Life Safety (LS), Collapse Prevention (CP), and Collapse damage states, were developed. These curves quantify the likelihood of damage progression under increasing deformation demands.
4. **Performance Assessment:** The application of the Capacity Spectrum Method, utilizing the structure's X-direction capacity and the NBC 105:2020 demand spectrum for soil type D, indicated a high degree of vulnerability. The analysis showed that performance points suggested that collapse prevention limits are exceeded even for moderate PGAs (~0.1g). Furthermore, collapse was predicted for design-level earthquakes (PGA > 0.15g), and instability was indicated for ground motions above a PGA of 0.21g.

The results unequivocally demonstrate the significant seismic risk faced by the traditional masonry building stock in Patan, as represented by the analyzed structure. The building's predicted performance falls short of the levels required to ensure life safety or prevent collapse under code-level seismic demands. The pronounced directional anisotropy observed underscores the necessity for multi-directional assessment in future vulnerability studies of such structures.

The fragility and capacity curves developed herein provide essential, context-specific tools. This can be utilized for quantitative risk assessment, prioritization of retrofitting efforts, and informed decision-making by engineers, conservation authorities, and policymakers in Patan. While acknowledging the limitations related to the analysis of a single representative building, the inherent assumptions of pushover analysis, and the incomplete nature of material data, this study establishes a robust baseline for understanding the seismic response of this critical building typology.

Future research should aim to expand the analysis to encompass a broader portfolio of buildings. The incorporation of nonlinear time-history analysis would allow for an enhanced and more detailed dynamic assessment. More extensive material testing, including the characterization of mortar and timber components, is also recommended. Furthermore, investigations into the effects of soil-structure interaction and an evaluation of the effectiveness of culturally sensitive retrofitting techniques would provide valuable insights. This work contributes vital knowledge towards the overarching goal of safeguarding Patan's invaluable cultural heritage and enhancing community resilience in the face of inevitable future seismic events.

Acknowledgements

The authors acknowledge the Department of Civil Engineering, Thapathali Campus, for providing the necessary support to conduct this study as a part of the BE final year project (2024/25). The authors also acknowledge the field support provided by Ms. Garima Boyaju for accompanying them in the geometrical measurement of the building. Further, the authors acknowledge the support and generosity provided by the house owner, Mrs. Ramila Bajracharya, for the detailed study of the building.

References:

Adhikari, R., Jha, P., Gautam, D., & Fabbrocino, G. (2019). Seismic strengthening of the Bagh Durbar heritage building in Kathmandu following the Gorkha earthquake sequence. *Buildings*, *9*(5), 128. https://doi.org/10.3390/buildings9050128

Applied Technology Council. (1996). Seismic evaluation and retrofit of concrete buildings (Report No. ATC-40). Redwood City, CA.

Barbat, A. H., Pujades, L. G., & Lantada, N. (2008). Seismic damage evaluation in urban areas using the capacity spectrum method: Application to Barcelona. *Soil Dynamics and Earthquake Engineering*, *28*(10–11), 851–865. https://doi.org/10.1016/J.SOILDYN.2007.10.006

Bashyal, J., Acharya, S., & Sundar Khadka, S. (2024). Seismic Assessment of an Old Historical Unreinforced Masonry Power House Building. *IOP Conference Series: Earth and Environmental Science*, *1385*(1). https://doi.org/10.1088/1755-1315/1385/1/012019

Combey, A., Tricoche, A., Audin, L., Gandreau, D., Benavente Escóbar, C., Bastante Abuhadba, J., Tavera, H., & Rodríguez-Pascua, M. Á. (2021). Monumental Inca remains and past seismic disasters: A relational database to support archaeoseismological investigations and cultural heritage preservation in the Andes. *Journal of South American Earth Sciences*, *111*. https://doi.org/10.1016/j.jsames.2021.103447

Endo, Y., & Hanazato, T. (2020). Seismic Analysis of a Three-Tiered Pagoda Temple Affected by the 2015 Gorkha Earthquake. *International Journal of Architectural Heritage*, *14*(3), 457–470. https://doi.org/10.1080/15583058.2018.1550534

Federal Emergency Management Agency (FEMA). (2000). *Prestandard and Commentary for the Seismic Rehabilitation of Buildings. Federal Emergency Management Agency*. https://www.academia.edu/88094745/FEMA_356_PRESTANDARD_AND_COMMENTARY_FOR_THE_SEISMIC_REHABILITATION

Fujiwara, T., Sato, T., Kubo, T., & Murakami, H. O. (1988). On the 21 August 1988 Earthquake in the Nepal-India border region.

Furukawa, A., Kiyono, J., Parajuli, R. R., Parajuli, H. R., & Toki, K. (2017). Evaluation of damage to a historic masonry building in Nepal through comparison of dynamic characteristics before and after the 2015 gorkha earthquake. *Frontiers in Built Environment*, *3*. https://doi.org/10.3389/fbuil.2017.00062

Gautam, D., & Rodrigues, H. (2021). Seismic Vulnerability of Urban Vernacular Buildings in Nepal: Case of Newari Construction. *Journal of Earthquake Engineering*, *25*(1), 43–64. https://doi.org/10.1080/13632469.2018.1498411

Gautam, D., Rodrigues, H., Bhetwal, K. K., Neupane, P., & Sanada, Y. (2016). Common structural and construction deficiencies of Nepalese buildings. *Innovative Infrastructure Solutions*, *1*(1), 1–18. https://doi.org/10.1007/S41062-016-0001-3/FIGURES/16

Hayes, G. P., Meyers, E. K., Dewey, J. W., Briggs, R. W., Earle, P. S., Benz, H. M., Smoczyk, G. M., Flamme, H. E., Barnhart, W. D., Gold, R. D., & Furlong, K. P. (2017). *Tectonic summaries of magnitude 7 and greater earthquakes from 2000 to 2015*. https://doi.org/10.3133/OFR20161192

IFRC. (2023). *OPERATION UPDATE Nepal | Karnali Earthquake.*

Jade, S., Mukul, M., Gaur, V. K., Kumar, K., Shrungeshwar, T. S., Satyal, G. S., Dumka, R. K., Jagannathan, S., Ananda, M. B., Kumar, P. D., & Banerjee, S. (2014). Contemporary deformation in the Kashmir-Himachal, Garhwal and Kumaon Himalaya: Significant insights from 1995-2008 GPS time series. *Journal of Geodesy*, *88*(6), 539–557. https://doi.org/10.1007/s00190-014-0702-3

Kathmandu, N. (2014). *National Population and Housing Census 2011 Economic Characteristics Tables Government of Nepal National Planning Commission Secretariat Central Bureau of Statistics*. www.cbs.gov.np

Khanal, K.N.(1997).*jngs, Source parameters estimation of the 1980 Bajhang Earthquake, far western Nepal.*

Lagomarsino, S., & Giovinazzi, S. (2006). Macroseismic and mechanical models for the vulnerability and damage assessment of current buildings. *Bulletin of Earthquake Engineering*, *4*(4), 415–443. https://doi.org/10.1007/s10518-006-9024-z

Lourenço, P. B., Fernandes, F. M., & Castro, F. (2010). Handmade clay bricks: Chemical, physical and mechanical properties. In *International Journal of Architectural Heritage* (Vol. 4, Issue 1, pp. 38–58). Routledge. https://doi.org/10.1080/15583050902871092

Motra, G. B., Sah, B. K., & Jha, P. (2021). Structural condition assessment and retrofitting of Shital Niwas building (presidential palace). *Progress in Disaster Science*, *10*. https://doi.org/10.1016/j.pdisas.2021.100174

Planning, N., & Secretariat, C. (2012). *National Population and Housing Census 2011 (National Report)*

National Planning Commission. (2015). *Nepal Earthquake 2015 Post Disaster Needs Assessment National Planning Commission Kathmandu 2015.*

National Statistics Office. (2023). *National population and housing census 2021 (national report)*. Government of Nepal. https://www.cbs.gov.np

https://censusnepal.cbs.gov.np/results/downloads/thematic?type=report

NBC 105. (2020). नेपाल राष्ट्रिय भवन संहिता Nepal National Building Code, नेपाल भूकम्प प्रतिरोधी भवन निर्माण ढाँचा (डिजाइन) Seismic Design Of Buildings In Nepal, नेपाल सरकार, सहरी विकास मन्त्रालय ।

UNESCO. (2018). *Kathmandu Valley. World Heritage List*. https://whc.unesco.org/en/list/121/

Upreti, B. N., & Yoshida, M. (2009). Seismic Hazard and Mitigation Activities in Nepal-with Emphasis on Kathmandu Valley. In *and the consequent tsunami)* (Vol. 2, Issue 1). Banda Achhe.

Vecchio, F. J., & C. M. P. (1986). The modified compression-field theory for reinforced concrete elements subjected to shear. *ACI Journal Proceedings*, *83(2)*, *219-231*.

Adhikari, A. S., Neupane, I., Maharjan, N., Dangol, K., & Paudel, S. (2025). *Performance Evaluation of Historical Masonry Structure*. *2*(1), 14–30.

Date, R., Building, U. M., Ayala, D. D., Bajracharya, S. S. R., & Brzev, S. N. (2003). *Traditional Nawari house in Kathmandu Valley*.

Dey, S., Panchanan, T., Mahavidyalaya, M., & Mahavidyalaya, D. (2015). *A Devastating Disaster : A Case Study of Nepal Earthquake and Its Impact on Human Beings*. *20*(7), 28–34. https://doi.org/10.9790/0837-20752834

Kiyono, J., Furukawa, A., Parajuli, H. R., Maskey, P. N., & Parajuli, R. R. (2017). *Vulnerability assessment of historic structures in kathmandu , nepal 2 . Method of Numerical Analysis*. *3091*(Abstract ID).

Lizundia, B., Shrestha, S. N., Bevington, J., Davidson, R., Jaiswal, K., Jimee, G. K., Kaushik, H., Kumar, H., Kupec, J., Mitrani-reiser, J., Poland, C., Shrestha, S., Welton-mitchell, C., Tremayne, H., & Ortiz, M. (2016). *M7 . 8 Gorkha , Nepal Earthquake on April 25 , 2015 and its Aftershocks* (Issue May).

Pan, Y., Wang, X., Guo, R., & Yuan, S. (2018). Seismic damage assessment of Nepalese cultural heritage building and seismic retro fi t strategies : 25 April 2015 Gorkha (Nepal) earthquake. *Engineering Failure Analysis*, *87*(February), 80–95. https://doi.org/10.1016/j.engfailanal.2018.02.007

Zentner, I., Gündel, M., & Bonfils, N. (2016). Fragility analysis methods : Review of existing approaches and application. *Nuclear Engineering and Design*. https://doi.org/10.1016/j.nucengdes.2016.12.021

Gautam, D., & Chaulagain, H. (2016). Structural performance and associated lessons to be learned from world earthquakes in Nepal after 25 April 2015 (M W 7 . 8) Gorkha earthquake. *EFA*, *68*, 222–243. https://doi.org/10.1016/j.engfailanal.2016.06.002